ADVANCED FUNCTIONAL MATERIALS
www.afm-journal.de

Pd–Cu Bimetallic Tripods: A Mechanistic Understanding of the Synthesis and Their Enhanced Electrocatalytic Activity for Formic Acid Oxidation

*Lei Zhang, Sang-Il Choi, Jing Tao, Hsin-Chieh Peng, Shuifen Xie, Yimei Zhu, Zhaoxiong Xie, and Younan Xia**

This article reports a facile synthesis of Pd-Cu bimetallic tripods with a purity over 90%. Two requirements must be met in order to form tripods: i) formation of triangular, plate-like seeds during the nucleation step and ii) preferential deposition of atoms onto the three corners of a seed during the growth step. In this synthesis, these requirements are fulfilled by adding $CuCl_2$ and KBr into an aqueous synthesis. Specifically, it is demonstrated that the Cu atoms resulting from underpotential deposition could greatly reduce the energy barrier involved in the formation of triangular seeds with planar defects because of the much lower stacking fault energy (41 mJ·m^{-2} for Cu vs 220 mJ·m^{-2} for Pd). The Br^- ions could strongly bind to the three {100} side faces of a triangular seed, forcing the Pd atoms to grow from the three corners of a seed to generate a tripod. When compared with commercial Pd black, the Pd-Cu tripods exhibited substantially enhanced catalytic activity toward the electro-oxidation of formic acid. This work offers a general strategy for the synthesis of nanocrystals with a tripod structure for catalytic applications.

1. Introduction

In recent years, fuel cells have received extensive attention owing to their many advantages, including high efficiency, high specific energy density, and low pollution.[1–3] Among various types of fuel cells, those based on formic acid are particularly well-suited for applications related to room-temperature power generation and portable electronics.[4,5] The performance of a direct formic acid fuel cell (DFAFC) is largely determined by the catalyst deposited on the anode for formic acid oxidation (FAO). Many studies have shown that Pd-based catalysts could be operated at high power densities, together with a remarkable capability to tolerate CO poisoning during the electro-oxidation of formic acid.[6–8] However, the low abundance of Pd in the Earth's crust and its high cost have created a major roadblock for the large-scale commercialization of DFAFCs. It is of great importance to reduce the loading of this precious metal in the catalyst by developing Pd-based nanocrystals with the highest possible activity toward FAO.

The activity of a catalyst is often determined by the structure or arrangement of atoms on the surface.[9,10] For face-centered cubic noble metals, most of their nanocrystals tend to take a polyhedral shape, such as truncated octahedron, cube, and octahedron.[11–14] Although these nanocrystals can be readily synthesized using a number of protocols, the {100} and/or {111} facets on their surfaces may not be the best candidate for FAO catalysis. As a matter of fact, the high-index facets on Pd nanocrystals with concave surfaces have been demonstrated with greater electrocatalytic activities toward FAO relative to the {100} and {111} facets.[15,16] In addition, our recent test indicated that the FAO activity of Pd right bipyramids was enhanced by 2.5 and 7.1 folds, respectively, relative to Pd nanocubes and commercial Pd black, owing to their {211} facets associated with the twin defects.[17] Since plate-like nanocrystals of Pd also contain planar defects such as twin planes and/or stacking faults similar to those of right bipyramids, they should be excellent candidates for FAO as well. However, due to the relatively high energy associated with stacking faults, the formation of Pd plate-like seeds is not favored by thermodynamics. The plate-like seed could only be prepared using a very slow reduction process.[12] For example, it was reported that Na_2PdCl_4 could be reduced by the hydroxyl end groups of PVP at an extremely slow rate to generate Pd nanoplates.[18]

L. Zhang, Dr. S.-I. Choi, H.-C. Peng, S. Xie, Prof. Y. Xia
The Wallace H. Coulter Department
of Biomedical Engineering
Georgia Institute of Technology and Emory University
School of Chemistry & Biochemistry
and School of Chemical and Biomolecular Engineering
Georgia Institute of Technology
Atlanta, Georgia 30332, USA
E-mail: younan.xia@bme.gatech.edu
L. Zhang, S. Xie, Prof. Z. Xie
State Key Laboratory for Physical Chemistry of
Solid Surfaces and Department of Chemistry
College of Chemistry and Chemical Engineering
Xiamen University
Xiamen, Fujian 361005, P. R. China
Dr. J. Tao, Dr. Y. Zhu
Condensed Matter Physics and Materials Science Department
Brookhaven National Laboratory
Upton, New York 11973, USA

DOI: 10.1002/adfm.201402350

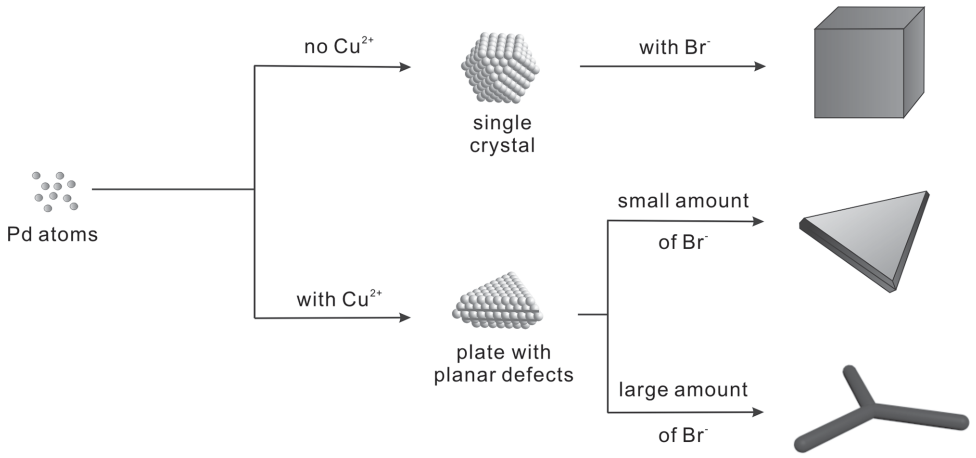

Figure 1. Schematic illustrations showing the evolution of Pd nanocrystals with different morphologies as controlled by both Cu^{2+} and Br^{-} ions.

The mass activity of a catalyst based on plate-like nanocrystals can be further enhanced by forming a tripod structure to increase the specific surface area. Over the past decade, a number of groups have successfully demonstrated the synthesis of tripods from several noble metals through anisotropic growth and further evaluated their use in various catalytic applications.[19–23] To this end, our group used Fe(III) and O_2 as an etchant to keep the reduction rate of a Pt precursor at a very low level to generate Pt seeds with branched arms. During the growth process, the reduction rate was slightly increased to induce the formation of Pt tripods and multipods.[19] Our group has also demonstrated a route to Rh tripods by selectively etching the edges of triangular plates formed in the early stage of a synthesis.[23] Yang and co-workers successfully demonstrated the synthesis of Pt tripods by decomposing $Pt(acac)_2$ at 160 °C in a mixture of 1,2-hexadecanediol, 1-hexadecylamine and diphenyl ether.[20] They obtained Pt tripods with uniform arm lengths and in high yields by controlling the molar ratio of $Pt(acac)_2$ to 1-adamantanecarboxylic acid at a specific value of 1:3. They also demonstrated, for the first time, that the stacking faults formed in the seed during the nucleation process were responsible for the formation of a tripod structure. In a recent publication, Huang and co-workers reported the synthesis of Pd tripods by reducing Na_2PdCl_4 with ascorbic acid (AA) in water at room temperature in the presence of $Cu(OAc)_2$ and cetyltrimethylammonium bromide (CTAB).[22] The percentage of tripods in their products was lower than 60%, typically with multipods as a major byproduct. The tripod was claimed to be "single-crystalline with their branches growing along the [111] and [200] directions." This assignment was contradictory to what was observed by Yang for the formation of Pt tripods. In addition, there was no explicit discussion on the possible roles played by the Cu species and the Br^{-} ions from CTAB in generating the tripods. They proposed that the formation of CuBr and CuCl was responsible for the low content (<6%) of Cu in the tripods. However, a large amount of Br^{-} or Cl^{-} ions in the solution should convert the insoluble CuX (X = Cl^{-} and Br^{-}) into soluble species such as $CuBr_2^{-}$ or $CuCl_2^{-}$. In this regard, the mechanism they proposed to account for the incorporation of Cu into the tripods also needs to be refined.

In this article, we report a simple and versatile route to the synthesis of Pd-Cu bimetallic tripods with a typical purity over 90% for the as-prepared samples. The success of this synthesis can be attributed to the formation of plate-like seeds with planar defects in the nucleation step and the preferential deposition of Pd onto the three corners of a seed during the growth process. Specifically, the slow reduction kinetics induced by the coordination between Br^{-} and Pd^{2+} ions favors the formation of plate-like seeds. The Cu atoms formed through underpotential deposition (UPD) further help reduce the energy barrier involved in the formation of plate-like seeds due to its much lower stacking fault energy than Pd (41 vs 220 $mJ \cdot m^{-2}$).[24,25] As illustrated in **Figure 1**, when no Cu^{2+} is introduced into the synthesis, single-crystal seeds of Pd will be formed in the nucleation step. These seeds then grow to nanocubes. With the introduction of Cu^{2+}, the low stacking fault energy of Cu promotes the formation of plate-like seeds at the early stage of a synthesis. The morphology of the final products is determined by the amount of KBr. Triangular plates with three {100} side surfaces are obtained when a relatively small amount of Br^{-} is added into the reaction solution. As the amount of KBr is increased, the three {100} side faces of each triangular seed will be blocked by the Br^{-} ions, and growth will only be allowed at the three corners to generate a tripod. Each tripod is comprised of a Pd-Cu alloy and the arms are grown along three <211> directions. Due to the tripod structure and the incorporation of Cu, the as-prepared tripods exhibit greatly enhanced activity toward the electro-oxidation of formic acid.

2. Results and Discussion

2.1. The Effect of $CuCl_2$ on the Morphology of Pd-based Nanocrystals

Figure 2 shows the formation of Pd-based nanocrystals with different morphologies as the amount of $CuCl_2$ added into the reaction solution was increased. Specifically, Pd nanocubes with an edge length of 18 nm were obtained in the absence of $CuCl_2$ (Figure 2a). In our previous work, we found that Br^{-} could selectively bind to the {100} facets of Pd nanocrystals,[26] leading to the formation of nanocubes.[14,27] When we introduced a small

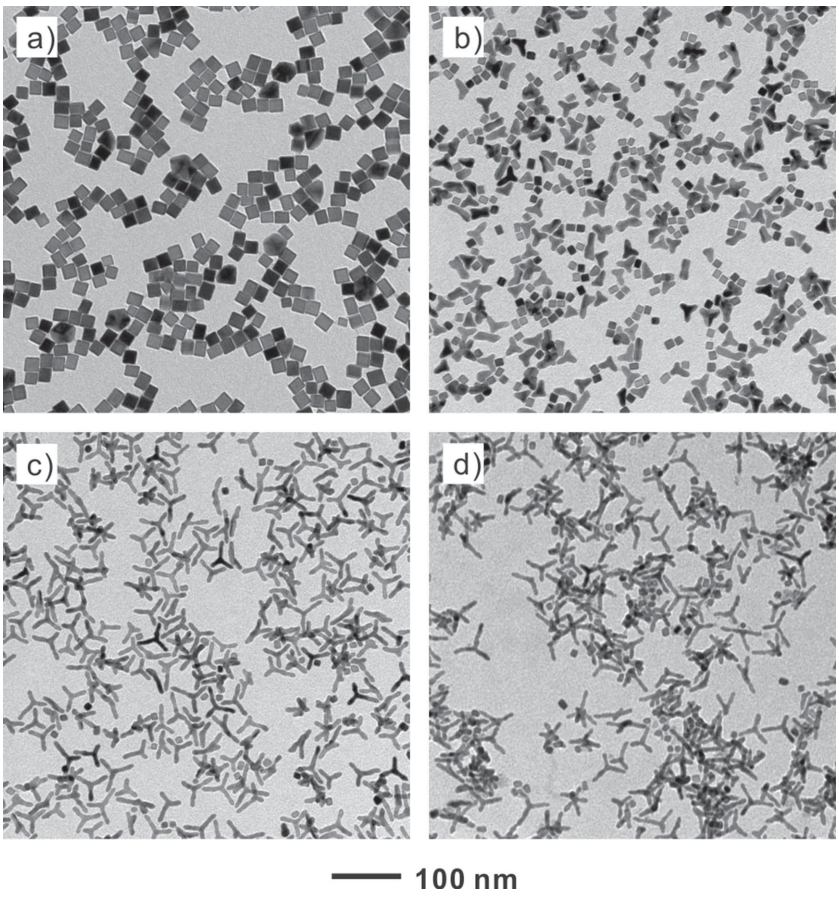

Figure 2. TEM images of Pd-based nanocrystals with different morphologies that were prepared using the standard procedure, with the introduction of different amounts of $CuCl_2{\cdot}2H_2O$: a) 0, b) 1, c) 3, and d) 5 mg.

amount of $CuCl_2$ at a Pd/Cu molar ratio of 11:1, the products became a mixture of nano-sized cubes and tripods (Figure 2b). In this case, the cubes were *ca*. 5 nm in edge length while the arms of the tripods were *ca*. 3 nm in length. When the amount of $CuCl_2$ was increased to a Pd/Cu molar ratio of 3.7:1, we obtained uniform tripods with arms of 50 nm in length (Figure 2c). Based on TEM images, the percentage of tripods in the as-obtained sample of such a synthesis was typically higher than 90%. ICP-MS measurement gives a mole fraction of 12.8% for Cu in the sample. When we further increased the amount of $CuCl_2$ to reach a Pd/Cu molar ratio of 2.2:1, the tripods showed little change in terms of size and uniformity (Figure 2d). However, the mole fraction of Cu in the product was increased to 20.5% as revealed by ICP-MS. When we further increased the amount of $CuCl_2$ to a Pd/Cu molar ratio of 1.6:1, most of the arms split into multiple forks and some small particles were also formed, as shown in Figure S1. These results indicate that the Cu species played a pivotal role in controlling the morphology of the Pd-based nanocrystals by participating in the nucleation and growth processes.

2.2. Characterization of the Pd-Cu Tripods

We first determined the crystal structure of the tripods shown in Figure 2c by X-ray powder diffraction (XRD). As shown in **Figure 3**a, the diffraction peaks of the as-prepared tripods appear between the peaks for pure face-centered cubic Pd and Cu, suggesting the formation of a Pd-Cu alloy. Using the least-square method, the lattice constant of the tripods was determined to be 0.3856±0.0002 nm. According to the Vegard's law, the lattice constant of an alloy is linearly correlated with its composition. From the lattice constant, a mole fraction of 12.0 ± 0.2% was derived for the Cu in the Pd-Cu tripods.[28] This composition is in good agreement with the value obtained from the ICP-MS analysis. Figure 3, b to e, shows TEM and HRTEM images of the tripods synthesized using the standard procedure (see Figure 2c). The lattice spacing of the tripod was measured to be 0.136 nm (Figure 3d), which is between the {220} lattice spacing of Cu (0.1278 nm, JCPDS NO. 04–0836) and that of Pd (0.1376 nm, JCPDS NO. 05–0681), confirming the formation of a Pd-Cu alloy. It should be pointed out that the 1/3(422) diffraction spots appeared in the FFT pattern viewed along the <111> direction, implying the presence of a (111) planar defect (stacking fault or twin plane) in the tripod.[18,29,30] From the HRTEM image and FFT pattern, we can conclude that each arm in the tripod was grown along the <211> direction. Figure 3f shows the HAADF-STEM image of one tripod. Elemental mapping obtained from the EDS analysis further confirms that the tripod is consisted of a Pd-Cu alloy.

We also analyzed the surface chemical composition of the Pd-Cu tripods shown in Figure 2c using X-ray photoelectron spectroscopy (XPS). As shown in Figure S2, we observed Pd 3d, Cu 2p, C 1s and Br 3d peaks in the survey spectrum. The peaks located at 340.5 and 335.2 eV can be assigned to elemental Pd $3d_{3/2}$ and Pd $3d_{5/2}$, respectively (Figure S2b). Two weak peaks at 931.6 eV and 951.1 eV were detected in the XPS spectrum (Figure S2c), which could be assigned to elemental Cu $2p_{3/2}$ and Cu $2p_{1/2}$, respectively. It should be pointed out that there was a minor shift for the peak positions relative to pure Pd and Cu because of a strong interaction between these two metals.[31–33] The XPS data suggests that the Cu atoms were incorporated into the Pd lattice to form an alloy.

2.3. Understanding the Role of Cu^{2+} in the Formation of Pd-Cu Tripods

Figure 4 shows the morphologies of the Pd-Cu alloy nanocrystals at different stages of a standard synthesis. As shown in Figure 4a, the products formed at t = 10 min were small particles of *ca*. 4 nm in size. The HRTEM image in the inset indicates that the particle had a triangular shape, together with three very short arms. As the synthesis proceeded, the seeds grew along three <211> directions and the length of the arms

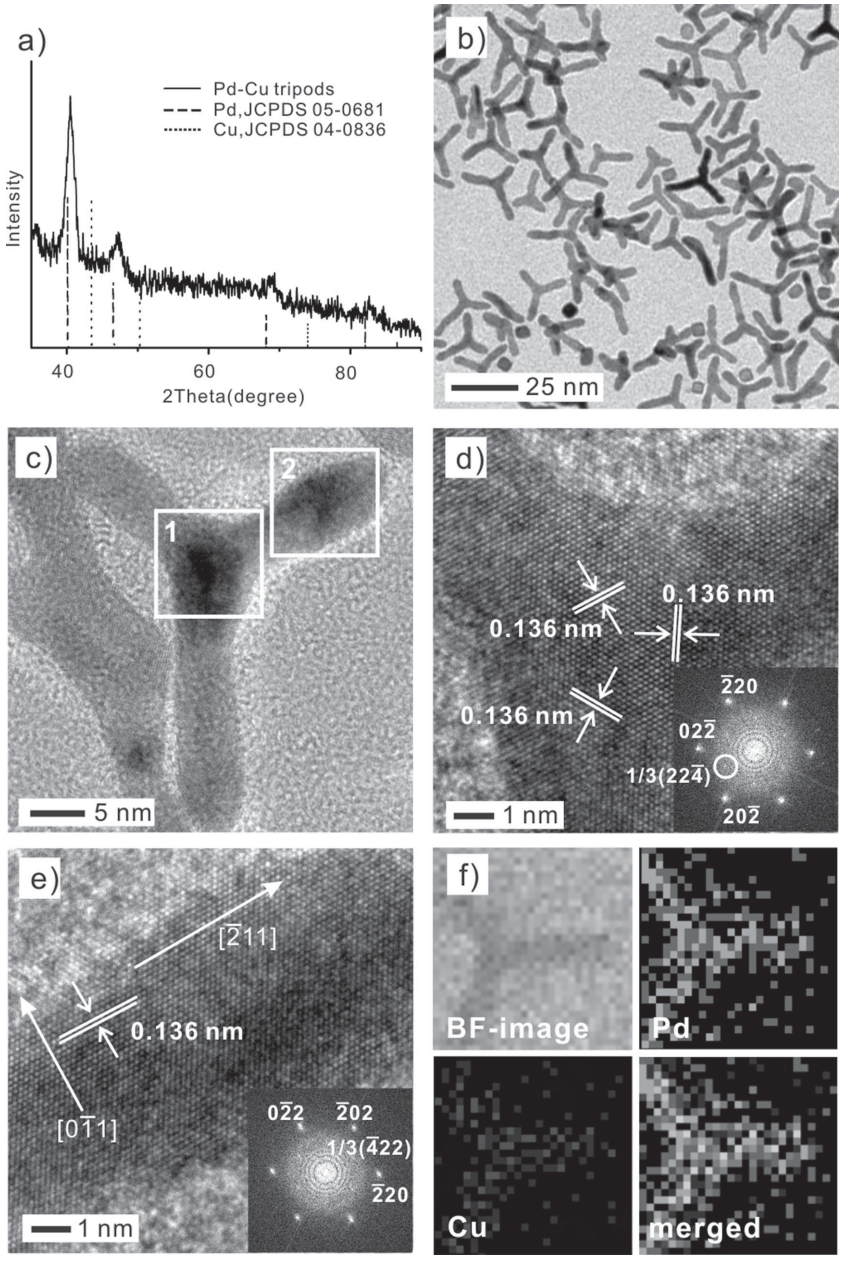

Figure 3. a) XRD pattern and b) a high-magnification TEM image of a typical sample of Pd-Cu tripods obtained using the standard procedure. c–e) High-resolution TEM images of an individual Pd-Cu tripod and the FFT patterns from the two regions marked in (c), respectively. f) EDX mapping of an individual Pd-Cu tripod.

was increased to 10 nm and 30 nm at t = 30 min and t = 1 h, respectively (Figure 4, b and c). Finally, when the reaction time was increased to 3 h, the arms of the tripods were further elongated to 50 nm in length. At t = 3 h, the growth was essentially terminated, and the dimensions of the tripods did not show any change when the reaction was prolonged. These results indicate that the tripods evolved from plate-like seeds with planar defects such as twin planes and stacking faults. We can also deduce the surface structure of the arms from the TEM analyses. For a hexagonal plate, the top and bottom flat faces should be bound by {111} planes while the six side faces are covered by a mix of {111} and {100} planes.[34,35] As illustrated in Figure S3a, the side faces of the arms were covered by {100} and {111} steps when the arms grew from three corners of a plate-like seed. Figure S3b shows the atomic arrangement on the side face characterized by alternation of {100} and {111} atom steps. Therefore, the side faces of the tripods can be assigned to {211} facets.

For the purpose of comparison, we also collected the initial products in the absence Cu^{2+}. As shown in Figure S4, the products obtained in the early stage of a synthesis were cubic seeds with a single-crystal structure when no Cu^{2+} was introduced. This result indicates that the seeds changed from a single-crystal to a plate-like structure in the presence of Cu^{2+}. This phenomenon can be understood from the difference in stacking fault energies between Pd and Cu. As we know, the plate-like seeds are covered by {111} facets with stacking faults along the vertical direction. In general, the total free energy of a plate-like seed should be much higher than a single-crystal seed due to the high lattice strain energy caused by defects. Since the stacking fault energy of Cu is much lower than that of Pd (41 vs 220 mJ·m^{-2}),[24,25] the stacking fault energy can be substantially reduced when a Pd-Cu alloy is involved.[36] In the present work, with the introduction of Cu^{2+}, the lower stacking fault energy of Cu helped reduce the energy barrier for the formation of plate-like seeds.

The standard redox potentials could help us understand how Cu was incorporated into the tripods. Owing to a larger stability constant for the coordination complex between Pd^{2+} or Cu^{2+} ions with Br^- as compared to Cl^-, the introduction of a great amount of Br^- into the solution should result in the formation of $PdBr_4^{2-}$ and $Cu(H_2O)_3Br^+$ complex ions *via* ligand exchange.[37,38] From the viewpoint of standard redox potential, $PdBr_4^{2-}$ ($PdBr_4^{2-} + 2e^- \rightleftarrows Pd + 4Br^-$ with $E^o = 0.56$ V) can be more easily reduced to its elemental form than $Cu(H_2O)_3Br^+$ ($CuBr^+ + 2e^- \rightleftarrows Cu + Br^-$ with $E^o = 0.34$ V). Meanwhile, $Cu(H_2O)_3Br^+$ can be reduced to CuBr by ascorbic acid ($CuBr^+ + e^- \rightleftarrows CuBr$ with $E^o = 0.64$ V). Although the K_{sp} of CuBr is only 6.27×10^{-9}, no CuBr precipitate was observed during our synthesis as it can be converted to $CuBr_2^-$ in the presence of a large amount of KBr.

An additional experiment was carried out using the standard procedure but in the absence of Na_2PdCl_4. No Cu particles was obtained. This result indicates that Cu atoms could not be formed through the direct reduction of $CuCl_2$ by AA in the absence of a Pd surface. The Cu UPD could only occur on the surface of a metal substrate at a higher redox potential than

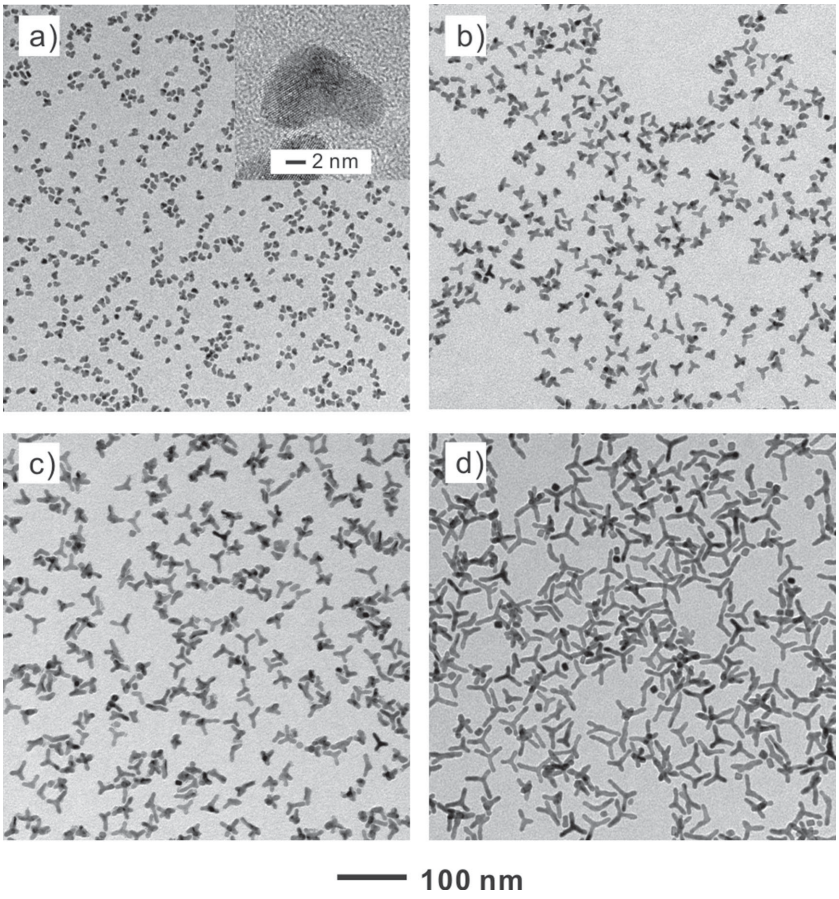

Figure 4. TEM images of the Pd-Cu tripods obtained using the standard procedure at different reaction times: a) 10 min, b) 30 min, c) 1 h, and d) 3 h, showing the evolution of morphology with time.

its standard reduction potential. The involvement of Cu UPD also offers a reasonable explanation for the incorporation of Cu into the tripods. Figure S5 schematically illustrates the process of Cu UPD involved in the growth of a nanocrystal. Initially, $PdBr_4^{2-}$ is preferentially reduced because of its high reduction potential. A monolayer of Cu UPD is then deposited on the Pd surface. Once a monolayer of Cu has been formed on the seed, there will be two different routes for the deposition of Pd onto the seed. The $PdBr_4^{2-}$ can be reduced to elemental Pd by AA or the elemental Cu deposited on the seed via a galvanic replacement reaction. When the reduction of $PdBr_4^{2-}$ by AA is very fast, some of the Cu atoms will be covered by the resultant Pd atoms and thus retained in the nanocrystal.

Based on the ICP-MS data, the mole fractions of Cu in the tripods at t = 10 min, 30 min, 1 h, and 3 h were 20.8%, 19.2%, 16.5% and 12.8%, respectively. This result indicates that the overall content of Cu in the tripods decreased along with the reaction time. This trend is a result of the two competing routes responsible for the formation of Pd atoms (Figure S5). Since the galvanic replacement reaction directly involves Cu, its rate is largely determined by the number of Cu atoms available on the surface. If the galvanic replacement reaction cannot be completed on time, the Cu atoms will be covered by the resultant Pd atoms and thus retained in the crystal lattice. In the early stage of a synthesis, the concentration of $PdBr_4^{2-}$ was high, so most of the Pd atoms would be formed through the reduction by AA and most of the Cu atoms formed by UPD would be retained in the nanocrystal. As the precursor was depleted, the reduction of Pd precursor by AA would be slowed down, giving the Cu atoms more chance to react with $PdBr_4^{2-}$ through the galvanic pathway. This can explain why the Cu content in the tripods was gradually reduced as the reaction was prolonged. Unless the Cu atoms formed through UPD could be oxidized back to the ionic format, the concentration of Cu ions in the reaction solution would drop with reaction time, also leading to a decrease for the incorporated Cu content.

2.4. The Effects of Br^- Ions and Other Parameters

We also carried out a set of experiments to elucidate the roles of KBr in the synthesis. When no KBr was added into a standard synthesis of Pd-Cu tripods, the precursor would be reduced at a greatly accelerated rate due to the involvement of $PdCl_4^{2-}$ rather than $PdBr_4^{2-}$. The product was dominated by triangular plates and multiply twined nanoparticles (**Figure 5**a). As shown in Figure 5b, only triangular plates were obtained when the amount of KBr was increased to 50 mg. The disappearance of multiply twinned nanoparticles can be attributed to the deceleration in reduction kinetics because of the addition of Br^-. The stronger coordination ability of Br^- relative to Cl^- helped decrease the reduction rate of the precursor, so only plate-like seeds were favored during the nucleation process. With the increase of KBr to 100 mg, tripods with arms of 20 nm in length were obtained (Figure 5c). The growth directions of the three arms were along three corners of the triangular plates. When the amount of KBr was increased to 200 mg as in the standard synthesis, tripods with arms of 50 nm in length were obtained (Figure 2c). When the amount of KBr was further increased to 300 mg, the length of the arms was increased to 100 nm (Figure 5d), albeit the uniformity of the sample deteriorated and some of the arms split into multiple forks. The increase in arm length can be attributed to the decrease in seed density formed in the solution due to the deceleration in reduction kinetics. Interestingly, the increase in the amount of KBr had a negligible impact on the nucleation process as both triangular plates and tripods evolved from the same plate-like seeds containing planar defects. It has been shown that Br^- could strongly bind to the {100} surface of Pd. When the amount of KBr was increased to a certain level, three of the {100} side faces of a triangular plate would be completely blocked by Br^- and the Pd atoms could only be deposited on the three corners of a plate-like seed to generate a tripod.

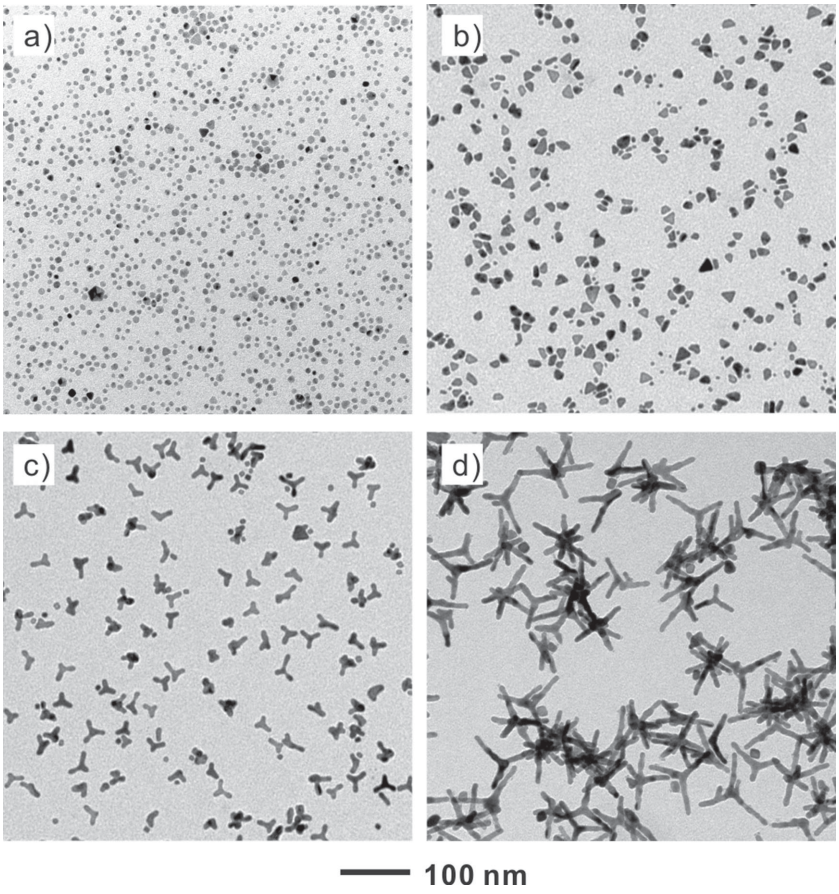

Figure 5. TEM images of Pd-Cu nanocrystals that were prepared using the standard procedure, except for the variation in the amount of KBr: a) 0, b) 50, c) 100, and d) 300 mg, respectively.

To examine how other parameters would influence the formation of Pd-Cu tripods, a set of control experiments based on the standard procedure were conducted. When we introduced the same molar amount of $CuSO_4$ instead of $CuCl_2$, the products were still nano-sized tripods (Figure S6a). Surprisingly, when we switched to $Cu(CH_3COO)_2$, the products were dominated by irregular particles, with very few tripods (Figure S6b). These results indicate that the anions could also affect the morphology of the final products. The obviously different results might originate from the variation in pH value as caused by the anions in the solution. Both Cl^- and SO_4^{2-} are the anionic groups of strong acids and they are not supposed to affect the pH value of a solution. In comparison, CH_3COO^- is the anionic group of a weak acid, the hydrolysis of acetate ions will increase the pH value of the solution. At a higher pH value, the reduction power of AA would become stronger and the reduction rate would be speeded up, leading to the formation of more irregular particles and fewer tripods.

We further investigated the possible role of other metal ions in inducing the formation of tripods. As shown in Figure S6c, irregular particles were obtained when Cu^{2+} was substituted by an equal molar amount of Fe^{3+}. In comparison, nanocubes were obtained when the metal ions were switched to Ni^{2+} (Figure S6d). These results further confirm the pivotal role of Cu^{2+} ions in inducing the formation of Pd-Cu tripods. In addition, the results shown in Figure S7 indicate that the formation of Pd-Cu tripods was highly sensitive to the type of Pd precursor. When $Pd(NO_3)_2$ instead of Na_2PdCl_4 was used, a mixture of tripods and irregular particles was produced (Figure S7a). When H_2PdCl_4 was employed as the precursor, plate-like particles with a size around 10 nm were obtained (Figure S7b). These results could be related to the difference in reduction kinetics since $Pd(NO_3)_2$ was reduced more easily than Na_2PdCl_4, whereas H_2PdCl_4 was more difficult to reduce by AA due to the involvement of a lower pH. These results indicate that the selection a Pd precursor with the proper reactivity is also critically important for the formation of tripods.

2.5. Selective Removal of Cu from the Tripods Through Oxidative Etching

The difference in reactivity between the two metals in an alloy allowed us to selectively dissolve the more reactive component using a proper etchant.[39–42] For example, our previous work demonstrated that the Ag contained in the walls of Au-Ag alloyed nanoboxes could be selectively removed using an aqueous solution containing $Fe(NO_3)_3$ or NH_4OH.[39] In the present work, we used HCl as an etchant to selectively remove Cu from the tripods at 90 °C. Because of its relative low standard redox potential, the Cu could be etched away without attacking the Pd. **Figure 6** shows TEM images of the products obtained by etching for 10 min with the introduction of 100, 250, 500 and 750 μmol of HCl, respectively. Interestingly, all the samples still displayed a tripod morphology after the etching with HCl. As shown in the insets of Figure 6, the width of the arms became thinner and thinner with the increase of HCl concentration. By carefully measuring the projected widths of the arms (we chose the thinnest portion of each arm as the arm width), the average arm widths of the tripods were determined to be 4.8, 4.1, 3.2, and 2.3 nm, respectively, for these four samples. The mole fractions of Cu in the products dropped to 12.2%, 10.5%, 8.2%, and 7.0% as revealed by ICP-MS. To determine whether the crystal structure of the tripods changed or not during etching, we also recorded XRD pattern from the etched tripods ($Pd_{93}Cu_7$, Figure 6d). As shown in Figure S8, each peak of the etched tripods was slightly shifted to a smaller angle relative to that of the original $Pd_{87}Cu_{13}$ tripods. The lattice constant of the etched tripods was determined to be 0.3871 ± 0.0002 nm. From the lattice constant, a mole fraction of $7.0 \pm 0.2\%$ was derived for the Cu in the Pd-Cu tripods, which was consistent with what was obtained from ICP-MS analysis. Therefore, the lattice of the etched tripods maintained an *fcc* structure and it also obeyed the Vegard's law. These results indicate that the Cu content in the tripods could be reduced through oxidative etching without changing the morphology and crystal structure.

We also investigated the etching process by sampling products from the reaction solution at different time points. We focused on

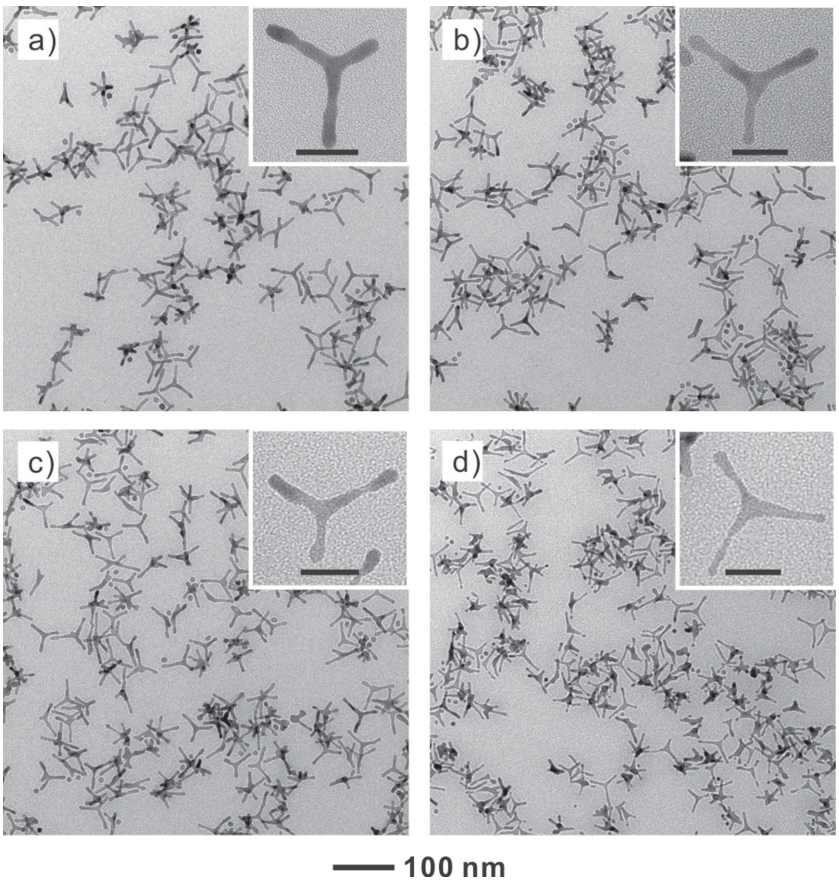

Figure 6. TEM images of the products obtained after etching for 10 min using different amounts of HCl as the etchant: a) 100, b) 250, c) 500, and d) 750 μmol, respectively, whereas the volume of the Pd-Cu tripods was fixed at 0.2 mL. Insets show TEM images at a higher magnification. (Scale bar: 30 nm.)

the cases shown in Figure 6a, which involved the introduction of 100 μmol of HCl. In this case, etching was very limited because of the low concentration of etchant. As a result, the width of the tripods was maintained at *ca.* 4.8 nm as the time was extended to 4 h (**Figure 7**, a–c). The Cu contents in the tripods were measured to be 11.5%, 10.8% and 9.1% at $t = 0.5$ h, 1 h and 4 h, respectively. When the etching time was extended to 24 h, the mole fraction of Cu in the product was further reduced to 7.5%. As shown in Figure 7d, the arms of the tripods also became shorter. This is because the diffusion rate of the atoms could be accelerated by heating up the sample to 90 °C. During the etching process, the relatively high specific surface area associated with an arm tended to force it to evolve into a shorter, more stable structure through atom diffusion. As a result, when the tripods were incubated at 90 °C for a long period of time, the atoms on the arms tended to diffuse to the center of each tripod, leading to the formation of shorter arms.

2.6. Electrocatalytic Activity of the Tripods Toward Formic Acid Oxidation

Since the Pd-Cu tripods have highly accessible {211} facets on the side faces, they are expected to be an excellent catalyst for various types of reactions. Here we used electrocatalytic oxidation of formic acid as a model system to characterize the catalytic activities of the Pd-Cu tripods with Cu mole fractions of 12.8% and 20.5%, corresponding to $Pd_{87}Cu_{13}$ and $Pd_{80}Cu_{20}$, respectively. For comparison, a commercial Pd black catalyst was used as a reference under the same conditions. All catalysts were directly deposited on glassy carbon electrodes. First, cyclic voltammograms (CV) were recorded in 0.10 M aqueous $HClO_4$ at a scanning rate of 50 $mV \cdot s^{-1}$ (Figure S9). For the Pd black, the intensity of current in the hydrogen desorption/adsorption region, which is directly proportional to the surface area of the catalyst, was much weaker relative to those of the Pd-Cu tripods. From the TEM image shown in Figure S10, it is clear that the particle size of the Pd black was much larger than the lateral dimensions of the tripods. **Figure 8** shows the CV curves of FAO recorded from the Pd-Cu tripods and the commercial Pd black, respectively. An aqueous solution containing 0.50 M HCOOH and 0.50 M $HClO_4$ was used. The curves for mass activity (per unit mass of Pd) of the catalysts were shown in Figure 8a. The anodic potential of FAO for the catalyst based on $Pd_{87}Cu_{13}$ tripods was peaked at 0.54 V (vs RHE) and the corresponding peak mass activity was 1.58 A/mg. The potential peaks for the $Pd_{80}Cu_{20}$ tripods and the commercial Pd black were positioned at 0.52 and 0.46 V with mass activities of 1.37 and 0.18 A/mg, respectively. Both of the Pd-Cu tripods performed better than the commercial Pd black, with the mass activity of the $Pd_{87}Cu_{13}$ tripods being 8.7 times that of the commercial Pd black. Figure 8b shows the current densities of the catalysts, which were normalized to ECSAs measured from the areas of hydrogen adsorption peaks in the CV measurements performed in 0.10 M $HClO_4$ electrolyte at a scanning rate of 50 $mV \cdot s^{-1}$ (Figure S9). The peak current densities for the $Pd_{87}Cu_{13}$ tripods, $Pd_{80}Cu_{20}$ tripods, and commercial Pd black were 5.51, 5.79 and 2.42 mA/cm^2, respectively. Both of the Pd-Cu tripods showed much higher oxidation current densities than the commercial Pd black. The highly accessible {211} facets on the side faces of a tripod structure is responsible for the enhanced activity for FAO. In addition, the enhanced electrochemical activity might be related to the density of Cu atoms on the surface of the tripod. A substantial proportion of Pd atoms on the surface of a tripod was required for the adsorption, dissociation, and activation of formic acid. However, the presence of Cu atoms on the surface could facilitate the oxidation of the adsorbed intermediates, as demonstrated in previous publications.[43,44] The amounts (13% and 20%) of Cu contained in our samples of Pd-Cu tripods were very close to the optimal amount (15%) of Cu reported in ref. 44 for Pd-Cu alloy nanoparticles. As a result, we only observed a minor difference between the catalytic activities of the $Pd_{87}Cu_{13}$ and $Pd_{80}Cu_{20}$ tripods.

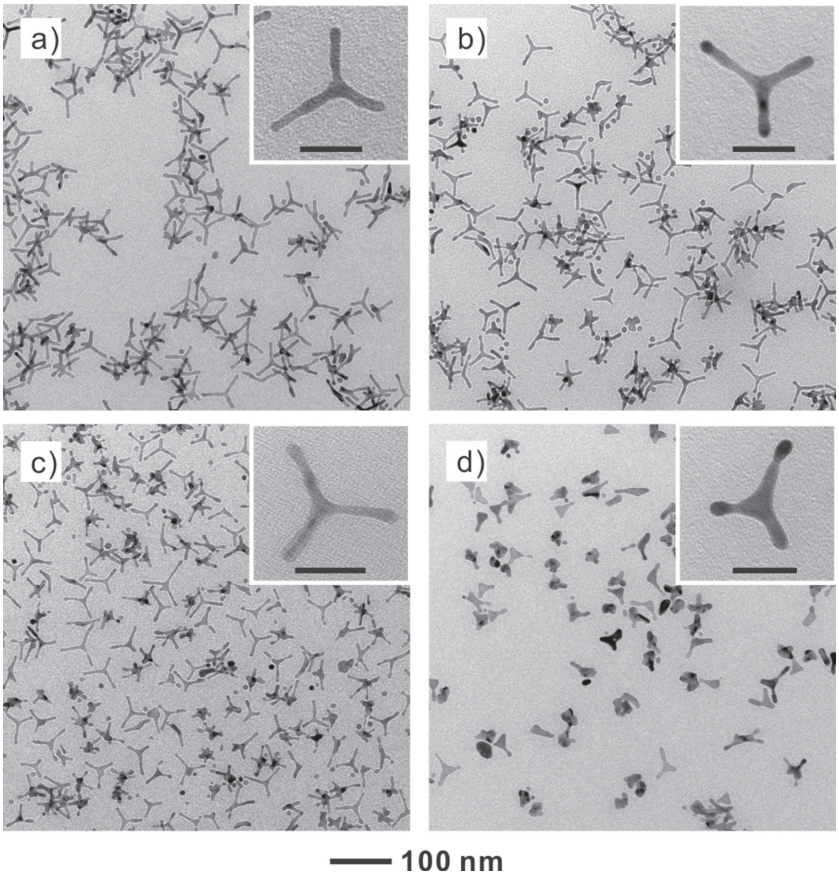

Figure 7. TEM images of the Pd-Cu tripods after etching with HCl for different periods of time: a) 30 min, b) 1 h, c) 4 h, and d) 24 h. Insets show TEM images at a higher magnification. (Scale bar: 30 nm.) In a typical etching experiment, 100 μmol of HCl was added into 0.2 mL of the as-obtained suspension of Pd-Cu tripods.

We also evaluated the catalytic stability of the as-prepared $Pd_{87}Cu_{13}$ and $Pd_{80}Cu_{20}$ tripods by benchmarking against the commercial Pd black. As shown in Figure S11, both samples of tripods showed higher stability compared to the Pd black. When comparing the $Pd_{87}Cu_{13}$ and $Pd_{80}Cu_{20}$ tripods, we found that the tripods with a lower Cu content showed higher stability during the electrochemical tests. This tend is understandable because the Cu atoms in a Pd-Cu tripods could be oxidized and leached out during an electrochemical test, which might cause the de-attachment of Pd atoms from the surface. From the results of both activity and stability, $Pd_{87}Cu_{13}$ tripods seem to be a good starting point for future refinement in searching for the most active and durable catalyst for FAO.

3. Conclusion

In summary, we have demonstrated a facile synthesis of Pd-Cu tripods with purity higher than 90%. The arms of the tripods were shown to grow along three <211> directions and their side faces were covered by highly accessible {211} facets. The samples obtained at different time points indicate that the tripods evolved from plate-like seeds with stacking faults or twin planes. Through XRD and EDS analysis, we also confirmed that the tripods were made of a Pd-Cu alloy. The incorporation of Cu in the tripod was attributed to the formation of Cu UPD layers on the Pd seed. The incorporated Cu atoms could help greatly reduce the energy barrier associated with the formation of planar defects. The formation of plate-like seeds was also facilitated by a slower reduction kinetics caused by the coordination between Br^- and Pd^{2+} ions. We also found that KBr played a key role in directing the growth of triangular, plate-like seeds into tripods during the growth step. The Br^- ions could strongly bind to the three {100} side faces, forcing the Pd atoms to be deposited on the three corners of a plate-like seed to generate a tripod. We have also tried to reduce the content of Cu in the tripods by selective etching. The Cu content was successfully reduced from 13% to 7% with the introduction of HCl as a wet etchant. When compared with the commercial Pd black, the Pd-Cu tripods exhibited substantially enhanced (almost eight

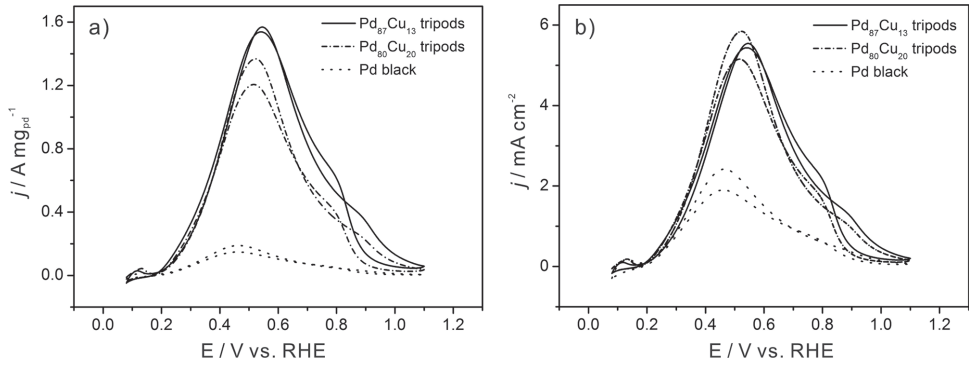

Figure 8. Cyclic voltammograms of the Pd-Cu tripods with different Pd to Cu ratios, together with that of commercial Pd black. The curve was recorded at room temperature in an aqueous solution containing 0.5 M HCOOH and 0.5 M $HClO_4$ at a sweeping rate of 50 mVs^{-1}. The current was normalized to the corresponding (a) mass of Pd and (b) ECSA, respectively. RHE: reversible hydrogen electrode.

folds per unit mass of Pd) catalytic activity toward the electro-oxidation of formic acid.

4. Experimental Section

Chemicals and Materials: Sodium palladium(II) tetrachloride (Na_2PdCl_4, 99.998%), palladium(II) chloride ($PdCl_2$), palladium(II) nitrate ($Pd(NO_3)_2$), copper(II) chloride dihydrate ($CuCl_2{\cdot}2H_2O$), copper(II) sulfate ($CuSO_4$), copper(II) acetate ($Cu(CH_3COO)_2$), iron(III) chloride ($FeCl_3$, 97%), nickel(II) chloride ($NiCl_2$), poly(vinyl pyrrolidone) (PVP, MW ≈ 55,000), L-ascorbic acid (AA), potassium bromide (KBr), and hydrochloric acid (HCl, 37%) were all obtained from Sigma-Aldrich and used as received. Commercial Pd black (99.9%) was obtained from Strem Chemicals. All aqueous solutions were prepared using deionized (DI) water with a resistivity of 18.2 MΩ·cm. A 10 mM H_2PdCl_4 solution was prepared by dissolving 0.1773 g of $PdCl_2$ in 10 mL of 0.2 M HCl solution.

Synthesis of Pd-Cu Tripods: In a standard procedure for the synthesis of Pd-Cu tripods with a composition of $Pd_{87}Cu_{13}$, PVP (35 mg), AA (20 mg), KBr (200 mg), and $CuCl_2{\cdot}2H_2O$ (3 mg) were dissolved in DI water (3 mL) and then placed in a vial and pre-heated at 80 °C in an oil bath under magnetic stirring for 10 min. Subsequently, Na_2PdCl_4 (19 mg) was dissolved in DI water (1 mL) and then added into the pre-heated solution using a pipette. The vial was capped and maintained at 80 °C for 3 h. The final products were collected by centrifugation, washed three times with DI water to remove excess PVP and salt ions, and then re-dispersed in DI water (4 mL). The Pd-Cu tripods with a composition of $Pd_{80}Cu_{20}$ were prepared using a similar procedure except that the amount of $CuCl_2{\cdot}2H_2O$ was increased from 3 mg to 5 mg.

Chemical Etching of the Pd-Cu Tripods: The $Pd_{87}Cu_{13}$ tripods were subjected to wet etching with HCl serving as the etchant. In a typical procedure, a specific amount of HCl (37%) was added into a vial containing 50 mg of PVP, 4 mL of DI water, 0.2 mL of an aqueous suspension of the as-prepared $Pd_{87}Cu_{13}$ tripods. The mixture was heated at 90 °C in an oil bath under magnetic stirring. After different periods of time, the products were collected by centrifugation, washed twice with DI water, and re-dispersed in DI water.

Electrochemical Measurements: The electrochemical measurements were performed at room temperature using a glassy carbon electrode connected to a CHI600E potentiostat (CH Instrument, Austin, TX). An Ag/AgCl electrode was used as the reference. The counter electrode was a Pt mesh (1 × 1 cm^2) connected to a Pt wire. All the potentials are presented with reference to the reversible hydrogen electrode (RHE). The glassy carbon electrode was carefully polished and washed with DI water before every experiment. Typically, 5 µl of an aqueous suspension (0.20 mg/mL) of the as-prepared Pd-Cu tripods or 10 µl of an aqueous suspension (0.20 mg/mL) of commercial Pd black was dropped onto the surface of the glassy carbon electrode with a geometric area of 0.07065 cm^2. Upon drying in an oven at 50 °C for 10 min, the electrode was covered with 5 µl of aqueous Nafion solution (0.05%) and allowed to dry in an oven at 50 °C for another 10 min. Then, plasma etching was applied for 10 min to remove the PVP on the surfaces of the Pd-Cu tripods. Electro-oxidation of formic acid was conducted in a solution containing 0.50 M $HClO_4$ and 0.50 M HCOOH at a sweeping rate of 50 $mV{\cdot}s^{-1}$. Electrochemical surface area (ECSA) was derived from the charges corresponding to the adsorption of hydrogen on the cyclic voltammogram (CV) obtained using 0.10 M $HClO_4$ at a scanning rate of 50 $mV{\cdot}s^{-1}$.

Instrumentation: Transmission electron microscopy (TEM) images were taken using a Hitachi H-7500 microscope operated at 80 kV. The samples were prepared by drop casting the dispersions of nanocrystal on carbon-coated Cu grids, followed by drying under ambient conditions. High-resolution TEM (HRTEM), high-angle annular dark-field scanning TEM (HAADF-STEM), and energy dispersive X-ray (EDX) analyses were performed using JEOL 2100F microscope (JEOL, Tokyo, Japan) operated at 200 kV. The X-ray photoelectron microscopy (XPS) data were collected using Thermo K-Alpha spectrometer with an Al Kα source. The samples for inductively coupled plasma mass spectroscopy (ICP-MS) analysis were prepared by dissolving the nanocrystals with concentrated HNO_3 and further diluted with 1% HNO_3 solution to a level of 100 ppb. The instrument was from Perkin-Elmer (NexION 300Q).

Supporting Information

Supporting Information is available from the Wiley Online Library or from the author.

Acknowledgements

This work was supported in part by a grant from the NSF (DMR-1215034) and start-up funds from the Georgia Institute of Technology. As visiting students from Xiamen University, L.Z. and S.X. were also partially supported by the China Scholarship Council (CSC). The work at BNL was supported by the U.S. Department of Energy, Basic Energy Sciences, by the Materials Sciences and Engineering Division under Contract No. DE-AC02–98CH10886 and through the use of CFN.

Received: July 15, 2014
Revised: August 24, 2014
Published online: September 16, 2014

[1] S. Srinivasan, R. Mosdale, P. Stevens, C. Yang, *Annu. Rev. Energy Environ.* **1999**, *24*, 281.
[2] A. S. Aricò, P. Bruce, B. Scrosati, J. M. Tarascon, W. V. Schalkwijk, *Nat. Mater.* **2005**, *4*, 366.
[3] U. B. Demirci, *J. Power Sources* **2007**, *169*, 239.
[4] C. Rice, S. Ha, R. I. Masel, P. Waszczuk, A. Wieckowsk, T. Barnard, *J. Power Sources* **2002**, *111*, 83.
[5] X. Yu, P. G. Pickup, *J. Power Sources* **2008**, *182*, 124.
[6] R. Larsen, S. Ha, J. Zakzeski, R. I. Masel, *J. Power Sources* **2006**, *157*, 78.
[7] R. Wang, S. Liao, S. Ji, *J. Power Sources* **2008**, *180*, 205.
[8] E. Antolini, *Energy Environ. Sci.* **2009**, *2*, 915.
[9] N. Tian, Z. Y. Zhou, S. G. Sun, Y. Ding, Z. L. Wang, *Science* **2007**, *316*, 732.
[10] M. Jin, H. Zhang, Z. Xie, Y. Xia, *Energy Environ. Sci.* **2012**, *5*, 6352.
[11] Y. Xiong, J. Chen, B. Wiley, Y. Xia, S. Aloni, Y. Yin, *J. Am. Chem. Soc.* **2005**, *127*, 7332.
[12] Y. Xia, Y. Xiong, B. Lim, S. E. Skrabalak, *Angew. Chem. Int. Ed.* **2009**, *48*, 60.
[13] W. Niu, L. Zhang, G. Xu, *ACS Nano* **2010**, *4*, 1987.
[14] M. Jin, H. Liu, H. Huang, Z. Xie, J. Liu, Y. Xia, *Nano Res.* **2011**, *4*, 83.
[15] J. Zhang, L. Zhang, S. Xie, Q. Kuang, X. Han, Z. Xie, L. Zheng, *Chem. Eur. J.* **2011**, *17*, 9915.
[16] M. Jin, H. Zhang, Z. Xie, Y. Xia, *Angew. Chem. Int. Ed.* **2011**, *50*, 7850.
[17] X. Xia, S.-I. Choi, J. A. Herron, N. Lu, J. Scaranto, H.-C. Peng, J. Wang, M. Mavrikakis, M. J. Kim, Y. Xia, *J. Am. Chem. Soc.* **2013**, *135*, 15706.
[18] Y. Xiong, I. Washio, J. Chen, H. Cai, Z.-Y. Li, Y. Xia, *Langmuir* **2006**, *22*, 8563.
[19] J. Chen, T. Herricks, Y. Xia, *Angew. Chem. Int. Ed.* **2005**, *44*, 2589.
[20] S. Maksimuk, X. Teng, H. Yang, *J. Phys. Chem. C* **2007**, *111*, 14312.
[21] B. Lim, Y. Xia, *Angew. Chem. Int. Ed.* **2011**, *50*, 76.
[22] Y. T. Chu, K. Chanda, P. H. Lin, M. H. Huang, *Langmuir* **2012**, *28*, 11258.
[23] S. Xie, H. Zhang, N. Lu, M. Jin, J. Wang, M. J. Kim, Z. Xie, Y. Xia, *Nano Lett.* **2013**, *13*, 6262.

[24] J. Cai, F. Wang, C. Lu, Y. Y. Wang, *Phys. Rev. B* **2004**, *69*, 224104.
[25] P. S. Branicio, J. Y. Zhang, D. J. Srolovitz, *Phys. Rev. B* **2013**, *88*, 064104.
[26] S.-H. Yoo, J.-H. Lee, B. Delleyb, A. Soon, *Phys. Chem. Chem. Phys.* **2014**, *16*, 18570.
[27] H.-C. Peng, S. Xie, J. Park, X. Xia, Y. Xia, *J. Am. Chem. Soc.* **2013**, *135*, 3780.
[28] A. R. Denton, N. W. Ashcroft, *Phys. Rev. A* **1991**, *43*, 3161.
[29] R. Jin, Y. Cao, C. A. Mirkin, K. L. Kelly, G. C. Schatz, J. G. Zheng, *Science* **2001**, *294*, 1901.
[30] Y. Xiong, A. R. Siekkinen, J. Wang, Y. Yin, M. J. Kim, Y. Xia, *J. Mater. Chem.* **2007**, *17*, 2600.
[31] X. Zhang, W. Wang, J. Liu, S. Sheng, G. Xiong, W. Yang, *Thin Solid Films* **2008**, *516*, 1849.
[32] N. Martensson, R. Nyholm, H. Calen, J. Hedman, B. Johansson, *Phys. Rev.* **1981**, *24*, 1725.
[33] A. Rochefort, M. Abon, P. Delichere, J. Bertolini, *Surf. Sci.* **1993**, *294*, 43.
[34] Z. L. Wang, *J. Phys. Chem. B* **2000**, *104*, 1153.
[35] Y. Xiong, J. M. McLellan, J. Chen, Y. Yin, Z. Y. Li, Y. Xia, *J. Am. Chem. Soc.* **2005**, *27*, 17118.
[36] I. R. Harris, I. L. Dillamore, R. E. Smallman, B. E. P. Beeston, *Phil. Mag.* **1966**, *14*, 325.
[37] S. Feldberg, P. Klotz, L. Newman, *Inorg. Chem.* **1972**, *11*, 2860.
[38] R. Näsänen, *Acta Chem. Scand.* **1950**, *4*, 816.
[39] X. Lu, L. Au, J. McLellan, Z.-Y. Li, M. Marquez, Y. Xia, *Nano Lett.* **2007**, *7*, 1764.
[40] E. C. Cho, C. M. Cobley, M. Rycenga, Y. Xia, *J. Mater. Chem.* **2009**, *19*, 6317.
[41] S. Xie, N. Lu, Z. Xie, J. Wang, M. J. Kim, Y. Xia, *Angew. Chem. Int. Ed.* **2012**, *51*, 10266.
[42] S. Xie, H.-C. Peng, N. Lu, J. Wang, M. J. Kim, Z. Xie, Y. Xia, *J. Am. Chem. Soc.* **2013**, *135*, 16658.
[43] K. H. Park, Y. W. Lee, S. W. Kang, S. W. Han, *Chem. Asian J.* **2011**, *6*, 1515.
[44] Z. Yin, W. Zhou, Y. Gao, D. Ma, C. J. Kiely, X. Bao, *Chem. Eur. J.* **2012**, *18*, 4887.